Title: Evaluating the sensitivity of forest structural diversity characterization to LiDAR point density

Authors: Elizabeth A. LaRue[1†], Robert Fahey[2], Tabatha L. Fuson[3], Jane R. Foster[4], Jaclyn Hatala Matthes[5], Brady S. Hardiman[6,7]

Affiliations:

[1]Department of Biological Sciences, The University of Texas at El Paso, El Paso, TX, USA (ealarue@utep.edu)

[2]Department of Natural Resources and the Environment and Center for Environmental Sciences and Engineering, University of Connecticut, Storrs, CT, USA (robert.fahey@uconn.edu)

[3]Environmental Science and Engineering, The University of Texas at El Paso, El Paso, TX, USA (Tlfuson@miners.utep.edu)

[4]Rubenstein School of Environment and Natural Resources, The University of Vermont, Burlington, VT, USA (jane.foster@uvm.edu)

[5]Department of Biological Sciences, Wellesley College, Wellesley, MA, USA (jmatthes@wellesley.edu)

[6]Forestry and Natural Resources, Purdue University, West Lafayette, IN, 47907

[7]Environmental and Ecological Engineering, Purdue University, West Lafayette, IN, 47907 (bhardima@purdue.edu)

[†]**Corresponding author:** ealarue@utep.edu

Preprints (www.preprints.org) | NOT PEER-REVIEWED | Posted: 23 December 2021 doi:10.20944/preprints202112.0390.v1

Abstract: Recent expansion in data sharing has created unprecedented opportunities to explore structure-function linkages in ecosystems across spatial and temporal scales. However, characteristics of the same data product, such as resolution, can change over time or spatial locations, as protocols are adapted to new technology or conditions, which may impact the data's potential utility and accuracy for addressing end user scientific questions. The National Ecological Observatory Network (NEON) provides data products for users from 81 sites and over a planned 30-year time frame, including discrete return Light Detection and Range (LiDAR) from an airborne observatory platform. LiDAR is a well-established and increasingly available remote sensing technology for measuring three-dimensional (3D) characteristics of ecosystem and landscape structure, including forest structural diversity. The LiDAR product that NEON provides can vary in point density from 2 – 25+ points/m^2 depending on instrument and acquisition date. We used NEON LiDAR from five forested sites to (1) identify the minimum point density at which structural diversity metrics can be robustly estimated across forested sites from different ecoclimatic zones in the USA and (2) to test the effects of variable point density on the estimation of a suite of structural diversity metrics and multivariate structural complexity types within and across forested sites. Twelve out of sixteen structural diversity metrics were sensitive to LiDAR point density in at least one of the five NEON forested sites. The minimum point density to reliably estimate the metrics ranged from 2.0 to 7.5 pt/$m^{2,}$ but our results indicate that point densities above 7-8 pt/m^2 should provide robust measurements of structural diversity in forests for temporal or spatial comparisons. The delineation of multivariate structural complexity types from a suite of 16 structural diversity metrics was robust within sites and across forest types for a LiDAR point density of 4 pt/m^2 and above. This study shows that different metrics of structural diversity can vary in their sensitivity to the resolution of LiDAR data and users of these open-source data products should consider the point density of their data and use caution in metric selection when making spatial or temporal comparisons from these datasets.

Keywords: Aerial laser scanning, Canopy structural complexity, Forest structure, National Ecological Observatory Network (NEON), Pulse density

Introduction:

Recent efforts that make ecological data freely available have created unprecedented opportunities to understand ecosystems across large spatial and temporal scales (Gewin 2016, Balch et al. 2020, Nagy and et al. 2021) but non-standard data resolution poses a challenge to using these datasets (Michener 2015). Ecological data sharing networks, such as the National Ecological Observatory Network (NEON), provide a source of large-scale data to anyone with internet access. Specifically, NEON offers a suite of biological, environmental, and remote sensing data products for a 30- year operational period (2018-2048) within the USA, spanning 81 sites and 20 ecoclimatic domains (Metzger et al. 2019). Despite protocols that were initially standardized for data collection at each site, rapid technological advances lead to increased data quality and resolution over time (Ouma 2016). While these changing data resolutions create benefits, they also pose potential challenges for making comparisons with ecological data across space and time (Reichman et al. 2011, Zipkin et al. 2021). Furthermore, given the rising popularity of open-source data networks, non-specialists are increasingly accessing these data products and might be unaware of technical considerations for data use and application (Huang et al. 2019, McCord et al. 2021b, 2021a). End users of these data streams require information and analyses focused on the impacts of changing data resolution on research outcomes and the utility of the data for answering scientific questions.

Discrete return LiDAR is one of the most widely available remote sensing technologies for measuring 3D aspects of ecosystem and landscape structure (Lefsky et al. 2002, Guo et al. 2021). The NEON Airborne Observation Platform (AOP) is equipped with an aerial discrete-return LiDAR, which collects data across the entire spatial footprint of each of the 81 sites that make up NEON (Krause and Goulden 2015). Data collection for these sites began as early as

2013, using the Optech Geminis (Optech ALTM Gemini) LiDAR sensor. This sensor has a maximum pulse repetition frequency (PRF) of 100 kHz and provides an average LiDAR point density of ~4 points/m^2 (Krause and Goulden 2015, NEON 2021b). Recently, in 2018, NEON AOP began using the Riegl LMS-Q780 sensor, with a PRF of 400 kHz and a higher return point density of double or more than that of the older instrument (NEON 2021b). However, higher resolution LiDAR data products are only available for a subset of sites from 2018 and onward, since the Optech Geminis sensors continue to be used at the remaining sites. Previous research has shown that NEON LiDAR data are useful for estimating the stand-level structural diversity of forest ecosystems (i.e. 3D arrangement of vegetation within ecosystems) (LaRue et al. 2019, 2020). However, efforts to characterize ecological patterns across space and time using NEON LiDAR data may be affected by variability in data resolution from these two sensors.

LiDAR resolution can influence the ability to resolve fine-scale structural attributes of ecosystems (Roussel et al. 2017, Pearse et al. 2019, Yu et al. 2020), because low density point clouds have reduced potential to resolve the spatial positioning of ecosystem components (Strunk et al. 2012). For example, use of lower resolution LiDAR data can lead to discrepancies in the mean and maximum canopy height by at least a meter (Roussel et al. 2017) and other vertical aspects of forested (Yao et al. 2014, Wilkes et al. 2015, Roussel et al. 2017, Yu et al. 2020) and non-forested land cover (Balsa-Barreiro and Lerma 2014). This presents a challenge when measuring ecosystem structural change through time so that measured values reflect true changes (e.g. geographic variation, Treitz et al. 2012; Wilkes et al. 2015) rather than noise associated with data resolution (Ruiz et al. 2014, Yao et al. 2014, Singh et al. 2015). Indeed, previous work has shown that LiDAR point density can influence values of forest structure metrics that represent cover, density, or volume of forest stands (González-Ferreiro et al. 2012, Jakubowski et al. 2013, de Almeida et al. 2019, Kamoske et al. 2021).

Past work addressing the impact of LiDAR point cloud resolution for characterizing structural metrics in forests have been largely focused on tree height or stem area for forestry applications (Strunk et al. 2012, González-Ferreiro et al. 2012, Treitz et al. 2012, Jakubowski et al. 2013, Roussel et al. 2017). Structural diversity is a promising tool for monitoring biodiversity and ecosystem function (Hakkenberg et al. 2016, Gough et al. 2019, LaRue et al. 2019), but consequently, there is a gap in our understanding of how varying LiDAR point cloud resolutions impact our ability to describe structural diversity metrics across forest types. Identifying the minimum point densities needed to reliably characterize univariate (Atkins et al. 2018, LaRue et al. 2020) or multivariate (Fahey et al. 2019) suites of structural diversity metrics could help facilitate inter-site and inter-annual comparisons using data of varying resolution and ensure repeatability in ecological monitoring efforts. Assessing the impact of point density on the characterization of a range of metrics is essential because, metrics are sensitive to different structural features within the forest canopy and thus may be differentially affected by variation in point densities. Furthermore, the degree of sensitivity might be influenced by forest type. Our goal was to use NEON LiDAR data to (1) identify the minimum point density at which structural diversity metrics can be robustly estimated across different forested sites in the USA and (2) to evaluate the effect of point density on delineation of multivariate forest structural complexity types.

Materials & Methods:

Structural diversity metrics from LiDAR

For this study, we chose NEON AOP LiDAR data collected with a high enough point density to allow for simulated point cloud thinning to produce a range of data resolution equivalent to that observed across the NEON sites and across aerial lidar acquisitions common in the literature. These data were accessed from the spatial extent of nine base (distributed) plots at each of five different NEON sites (Table 1) and had a point density of at least 25 pt/m^2

Preprints (www.preprints.org) | NOT PEER-REVIEWED | Posted: 23 December 2021 doi:10.20944/preprints202112.0390.v1

within the 40 x 40 m area. Within the NEON sampling design, a series of plots, called base or distributed plots, are where multiple data products are collected and is therefore the spatial grain size commonly used by many NEON data users; therefore, we extracted LiDAR from a subset of these plots that met the minimum data resolution for this study. We randomly thinned the LiDAR data at these 45 plots to eight different point densities ranging from 2 to 25 pt/m^2 (Fig. 1) and used the thinned data to estimate 16 structural diversity metrics (Table 2). Years of data collection for sites included ABBY 2018, GRSM 2018, STEI 2019, UKFS 2019, and 2020 UNDE.

Of the NEON AOP LiDAR data products available, we obtained the level 1 discrete return LiDAR (Product No. DP1.30003.001) (NEON 2021a), corrected each plot's point cloud for elevation, and randomly thinned the plots to the eight different point densities. The 1 km^2 tiles of LiDAR that is provided by NEON, were downloaded for the selected plots using the neonUtilities R package (National Ecological Observatory Network 2020). This data is collected during peak growing season greenness (Krause and Goulden 2015); the data and specific details about data collection and sensor specs are found on the NEON Data Portal Website (https://www.neonscience.org/). Following data acquisition, an 80 by 80 m buffer area was clipped around the base plot centroid and each plot was visually checked to ensure that there were no large gaps in the LiDAR data coverage. Clusters of atmospheric and ground outliers were filtered by removing points six standard deviations above and below the mean height. Isolated point outliers were then identified and filtered using the classify_noise function with the isolated voxels filter algorithm (points that had zero neighboring points in a 3 x 3 x 3 window) in the lidR v. 3.1.2 R package (Roussel and Auty 2018). The 80 x 80 m buffer area was then corrected for elevation using a Delaunay triangulation before being clipped to the 40 x 40 m base plot area. Each plot was then visually inspected to ensure that outliers were successfully removed. Finally, the processed point cloud for each plot was randomly thinned (i.e., points

Preprints (www.preprints.org) | NOT PEER-REVIEWED | Posted: 23 December 2021 doi:10.20944/preprints202112.0390.v1

randomly selected until the specified point density was reached) from the original processed point cloud to 8 different point densities (Fig. 1): 2, 4, 6, 8, 10, 15, 20, and 25 pt/m^2. The random thinning process was repeated for each point density and plot five times to mimic the random locations that the laser pulse would hit objects during fly over.

Sixteen structural diversity metrics from five categories that describe the height, cover and openness, density, internal heterogeneity, and external heterogeneity of vegetation in the canopy were calculated (Table 2) (patterned after LaRue et al. 2020). All metrics, unless specified otherwise, were calculated using functions from the lidR v.1.3.2 R package (Roussel and Auty 2018). Rumple (rumple_index function) and DGF were calculated from a 1 m^2 grid canopy height model from all returns (grid_canopy function) and for which points below 3 m were converted to a value of zero. MOCH and top rugosity were calculated from a second 1 m^2 grid canopy height model for which points below 0.5 m were removed (ground points). After filtering out points below 0.5 m, we calculated the following metrics from the point cloud: using the leafR package and functions listed in parentheses (Roberti et al. 2019) height quantiles, SD(ht), and CV(ht) (preceding functions all cloud_metrics function), SD(SD(ht)) (grid_metrics function), GFP (gap_fraction_profile function), VAI (LAD function), and VCI (VCI function). FHD (FHD function) and the Gini index (GC function) were estimated with the leafR R package (Roberti et al. 2019).

Analyses

We used segmented regressions to determine if there was a change point in the structural diversity metric values with increasing LiDAR point density at each plot. The presence of a difference in the slope of the line before and after the break indicated that the value of metrics varied across LiDAR point densities. Each segmented regression analysis included the eight-point densities for a specific plot and the five replicates for each density ($N_{Replicates/Density}$ = 5 for a total of N_{Points} = 40). When structural diversity metrics do not change as point density

Preprints (www.preprints.org) | NOT PEER-REVIEWED | Posted: 23 December 2021 doi:10.20944/preprints202112.0390.v1

increases, the relationship is flat and produces no change point. When the relationship is nonlinear, we assume that the change point indicates when the metric is stable with respect to changes in point density. Assuming two segments, we used a pseudo score statistic test to determine when segmented regression was need with the segmented R package (Muggeo 2008). The p-value for each pseudo score test was corrected for multiple comparisons using the false discovery rate (N_{Tests} = 720). If the pseudo score statistic test had an $\alpha < 0.05$ after correcting for multiple comparisons, then we employed segmented regression to determine the density value of the two-segment change point in the linear slope. We used an initial change point estimate of 8 pt/m^2. The mean and standard deviation of the change point in the linear slope was calculated for each of the nine plots across each site to summarize the average change point at different forested sites and variation of change points in plots within sites (Table 3). If the pseudo score statistic test determined that segmented regression was not needed (insignificant), then a value of 2.0 pt/m^2 was assigned to that plot in the calculation of the average and standard deviation of the change point for that site.

We assessed whether variation in LiDAR point density resulted in variable delineation of plots into multivariate structural complexity types (Fahey et al. 2019) using multivariate analyses with the 16 structural metrics. We used non-metric multidimensional scaling (NMS) ordination on plot-level data sets of one plot replicate from each of the eight LiDAR point densities. NMS ordinations were conducted in PC-ORD v.5.31 (McCune and Mefford 2006) with Sorensen's distance measure, the ''slow-and-thorough'' setting, and 250 runs of real data and 250 Monte Carlo randomizations for solution robustness testing (McCune and Grace 2002). Metrics were standardized relative to the maximum value to scale metrics before ordination was conducted. Hierarchical agglomerative clustering in PC-ORD, using Ward's method and Euclidean distance measures (McCune and Grace 2002), was used to delineate plots into canopy structural complexity type groupings following the method of (Fahey et al. 2019) but here clusters (types)

Preprints (www.preprints.org) | NOT PEER-REVIEWED | Posted: 23 December 2021 doi:10.20944/preprints202112.0390.v1

were based on structural variation in our own data. The optimal cluster group level was assessed using indicator species analysis and mean p-values derived across all metrics for each level (McCune and Grace 2002); the clustering level with the lowest mean p-value was used as the optimal number of groups. We then evaluated the group membership of plots to assess whether the designation of structural type for each plot changed across LiDAR point densities.

Results:

Minimum LiDAR point density for estimating structural diversity across forested sites

Four structural diversity metrics, from three categories, remained stable across LiDAR point densities for all plots at each of the 5 sites. Of these, two were from the height category and the remaining two were from the density and internal heterogeneity categories. These included the height metrics of Q25 and Q75, the density metric of VAI (Table 3, Fig. 2, Table S1), and the internal heterogeneity metrics of SD(ht) (Table 3, Fig. 3, Appendix 1: Table S1).

There were 12 structural diversity metrics that varied as sample point density increased, with seven stabilizing between 2.1 and 4.7 pt/m^2 and five metrics stabilizing between 5.1 and 7.5 pt/m^2. The metrics that stabilized at low to moderate change point density (2.1 to 4.7 pt/m^2) included q50 and q100 metrics from the height category; GFP from cover and openness; VCI, CV(ht), FHD, and Gini Index from internal heterogeneity. The metrics that required higher point densities to stabilize (5.1 to 7.5 pt/m^2) were MOCH from the height category; DGF from openness and cover; rumple and top rugosity from external heterogeneity; and SDSD(ht) from internal heterogeneity.

Several metrics, like FHD, fluctuated between plots within sites and caused change point variation between sites. The change point in segmented regressions for a structural diversity metric had an average and standard deviation that varied by site. FHD had the highest standard

Preprints (www.preprints.org) | NOT PEER-REVIEWED | Posted: 23 December 2021 doi:10.20944/preprints202112.0390.v1

deviation in change point across sites. Most other six metrics had lower standard deviations at a site, with many sites having no significant change point at any plot (i.e. metric value was stable across LiDAR point density). In general, for all metrics and plot combinations, when a change point was found, the change point was not more than 10 pt/m^2, except for three plots with Q100 (STEI_046 at 16.7) and FHD (ABBY_025 at 13.7 and ABBY_029 at 13.5) (Appendix 1: Table S1).

The effect of LiDAR point density on delineating structural complexity types

At all LiDAR point densities, five clusters representing structural complexity types were delineated across the NEON study sites (Fig. 4), but at the lowest point density, cluster assignment for several plots differed from the consistent assignment pattern observed across the higher point densities. Variation in the first NMS axes (59.7%) was explained predominantly by VCI and q100 structural diversity metrics, with the structural complexity types split as tall, heterogeneous canopies or short, homogeneous canopies. The variation in the second NMS axis (39.8%) was explained by FHD and Gini Index metrics with structural complexity types split as multilayered, less skewness in height distribution or vice versa. Groupings were identical for densities of 4-25 pt/m^2 (Fig. 4c), but there were 8 plots that were placed into different clusters at 2 pt/m^2, including plots from sites STEI, UKFS, GRSM, and ABBY. Overall, the delineation of structural complexity types was robust within sites and across forest types for a suite of 16 structural diversity metrics and LiDAR point density of 4 pt/m^2 and above.

Discussion:

We identified metrics of structural diversity that were not sensitive to LiDAR point density, which could be utilized by LiDAR users to characterize forest structural diversity with less concern for data resolution impacts on assessment of temporal or spatial patterns. Of the 16 metrics evaluated here, four showed little to no variation across LiDAR point density. These

Preprints (www.preprints.org) | NOT PEER-REVIEWED | Posted: 23 December 2021 doi:10.20944/preprints202112.0390.v1

metrics included descriptors from height, density, and internal heterogeneity categories and their stability even at low point densities suggests that these metrics could be suitable for making accurate multi-temporal or cross-site comparisons between LiDAR datasets, regardless of instrumentation or instrument parameterization within the range of 2 – 25 pt/m^2. By focusing on these four metrics, it is probable that any temporal variation detected is due to real changes in structural diversity rather than noise. Previous studies relating point density to vertical forest structure found similar results with metrics associated with height and density, with some metrics even improving under lower densities (Treitz et al. 2012, Jakubowski et al. 2013) and recommended that metrics unaffected by low-density point clouds could be calculated with less data, regardless of instrumentation.

The remaining three quarters of structural diversity metrics in our study were sensitive to the point density of LiDAR, such that users of low-resolution LiDAR (e.g. NEON or USGS 3DEP with average point densities ranging well below 8 pt/m^2) should carefully consider the use of these metrics in temporal or spatial comparisons of forest structural diversity. On average values of structural diversity metrics across a range of forested NEON sites became stable at or above a LiDAR point density of 8.1 pt/m^2 when plots were averaged within a site. Our study therefore indicates that for the forest types studied here, LiDAR datasets with a resolution of at least ~ 8 pt/m^2 should provide the most robust temporal and spatial comparisons of forest structural diversity. Similarly, Yao *et al.* (2014) found that once LiDAR achieved 10 pt/m^2, that any advantage of having a higher data resolution for individual tree detection plateaued. However, other studies that used pulse density to quantify LiDAR resolution found that metrics that require an internal view of the canopy were not well resolved with a low resolution (e.g. LAI, subcanopy cover, Jakubowski et al. 2013, de Almeida et al. 2019). For example, categories of structural diversity metrics that describe the internal heterogeneity of canopies may be most susceptible to low point densities because the subcanopy often has fewer data points due to occlusion (LaRue et al. 2020).

Preprints (www.preprints.org) | NOT PEER-REVIEWED | Posted: 23 December 2021 doi:10.20944/preprints202112.0390.v1

The stable point density was often lower (2.1 to 8.1 pt/m^2) than the maximum 8.1 pt/m^2 site average for several structural diversity metrics, which can be explained by the way metrics are calculated. The five metrics that had stable change points at higher densities (average across sites 5.1 – 7.5 pt/m^2) were spread across structural diversity categories but were calculated through subsetting the point cloud into voxels. In contrast, the six metrics that had an average change point on the lower end of the (2.1 – 4.7 pt/m^2) were calculated by using points across the entire point cloud (no spatially explicit separation or subsetting the data into voxels). A lower point cloud resolution likely causes variation in specific locations (Roussel et al. 2017) for height and area in ground surface and sparse cover (Wilkes et al. 2015), such that metric values calculated using a voxelization or grid (canopy height model) have lowered stability. In summary, vertical stratification of height across a plot may be less sensitive to lower point densities than spatial stratification of points across a plot.

There was variation in the change point identified by the segmented regressions at individual plots within sites for the same metric, which might be explained by differential environmental heterogeneity and the impact of heterogeneous disturbances (both natural and anthropogenic) that affect the structural heterogeneity of the forest across scales. For example, ABBY, located within the western foothills of the Cascade Range, has a long history of logging resulting in a dynamic forested landscape with a mosaic of age classes and resulting structural signatures of disturbance across the plots within this site (NEON 2021c). Similarly, UNDE and STEI sites were heavily logged as recent as 1960 and 2005, respectively, with both first and secondary growth patterns found across the sites. The GRSM site located in the Smoky Mountains of southeastern Tennessee had wildfires in 2016 that burned over more than 10,000 acres including areas within the study region. Indeed, structural diversity is known to vary differently in disturbed sites, including at GRSM after the 2016 fire (Atkins et al. 2020). It is likely that these landscape disturbances are driving variation in metric values between plots and sites

Preprints (www.preprints.org) | NOT PEER-REVIEWED | Posted: 23 December 2021 doi:10.20944/preprints202112.0390.v1

and certain structural configurations may be more sensitive to low point density LiDAR data (i.e. some metrics and canopy configurations cannot be accurately measured with low resolution data).

To monitor forest structural changes in response to disturbance and succession, a multivariate approach focused on categorizing forest stands into structural complexity types based on variation along axes such as maximum canopy height and internal heterogeneity of vegetation arrangement may be useful (Franklin and Hemstrom 1981, Spies and Franklin 1988, Fahey et al. 2019, Atkins et al. 2020). However, results from this study suggest that LiDAR data used for this type of analysis should have a minimum point density to ensure reproducibility of structural type categorization. Ruiz *et al.* 2014 found that a multivariate approach of structural indices from aerial LiDAR achieve greater predictive ability of forest inventory variables such as biomass and cover over a point density of 1 pt/m^2, but that the marginal benefit of increasing point density declined above 5 pt/m^2 (Ruiz et al. 2014). The identification of forest structural complexity types among plots and sites was robust down to a LiDAR density of 4 pt/m^2. Therefore, our results suggest that users wanting to describe the structural diversity of canopies in their area of interest along a spectrum of forest structural complexity types using multivariate analyses (Fahey et al. 2019) can do so confidently with NEON LiDAR data of 4 pt/m^2 and above. Furthermore, the discrepancies in categorizing plots (8 out of 45) into structural complexity types at the lowest data resolution occurred in the middle of the first NMS axis, such that these plots exhibited a moderate canopy height and internal heterogeneity. LiDAR of 2 pt/m^2 is likely to have fewer points that reach the inner canopy or subcanopy and considerable noise in point placement. However, our results indicate that relatively low-resolution LiDAR may be suitable for temporal comparisons of changing canopy structural complexity types. For example, the use of LiDAR to exhibit changes in structural complexity types that are indicative of successional stages or species compositions in response to disturbance or global change

might be important for characterizing forest change over the 30-year time span of NEON monitoring (Metzger et al. 2019, Dodds et al. 2021).

Acknowledgements: Funding was provided by NSF DEB award #1926538 to BSH and #1924942 to EAL and BSH, #2106103 to EAL, #1926442 to RF, and #1926454 to JHM.

Author Contributions: EL conceived the original idea, conducted the analyses, and wrote the initial draft. RF conducted the multivariate analyses. All authors contributed to manuscript editing and approved the final version.

Data availability: LiDAR data is available through the neonscience.org data portal. R code that was used to process the LIDAR and generate data and analysis results can be obtained at https://github.com/lizlarue/NEONLidarFSDPointDensity.

Literature Cited:

de Almeida, D. R. A., S. C. Stark, G. Shao, J. Schietti, B. W. Nelson, C. A. Silva, E. B. Gorgens, R. Valbuena, D. de A. Papa, and P. H. S. Brancalion. 2019. Optimizing the remote detection of tropical rainforest structure with airborne lidar: Leaf area profile sensitivity to pulse density and spatial sampling. Remote Sensing 11:92.

Atkins, J. W., G. Bohrer, R. T. Fahey, B. S. Hardiman, T. H. Morin, A. E. L. Stovall, and C. M. Gough. 2018. Quantifying vegetation and canopy structural complexity from TLS data using the forestr r package. Methods in Ecology and Evolution 9:2057–2066.

Atkins, J. W., B. Bond-Lamberty, R. T. Fahey, L. T. Haber, E. Stuart-Haëntjens, B. S. Hardiman, E. LaRue, B. E. McNeil, D. A. Orwig, A. E. L. Stovall, J. M. Tallant, J. A. Walter, and C. M. Gough. 2020. Application of multidimensional structural characterization to detect and describe moderate forest disturbance. Ecosphere 11:e03156.

Balch, J. K., R. C. Nagy, and B. S. Halpern. 2020. NEON is seeding the next revolution in ecology. Frontiers in Ecology and the Environment 18:3.

344 Balsa-Barreiro, J., and J. L. Lerma. 2014. Empirical study of variation in lidar point density over
345 different land covers. International Journal of Remote Sensing 35:3372–3383.
346 Dodds, W. K., K. C. Rose, S. Fei, and S. Chandra. 2021. Macrosystems revisited: challenges
347 and successes in a new subdiscipline of ecology. Frontiers in Ecology and the Environment
348 19:4–10.
349 Fahey, R. T., J. W. Atkins, C. M. Gough, B. S. Hardiman, L. E. Nave, J. M. Tallant, K. J.
350 Nadehoffer, C. Vogel, C. M. Scheuermann, E. Stuart-Haëntjens, L. T. Haber, A. T. Fotis, R.
351 Ricart, and P. S. Curtis. 2019. Defining a spectrum of integrative trait-based vegetation
352 canopy structural types. Ecology Letters 22:2049–2059.
353 Franklin, J. F., and M. A. Hemstrom. 1981. Aspects of succession in the coniferous forests of
354 the Pacific Northwest. Pages 212–229 *in* D. C. West, H. H. Shugart, and D. B. Botkin,
355 editors. Forest succession: Concepts and application. Springer-Verlag, New York.
356 Gewin, V. 2016. Data sharing: An open mind on open data. Nature 529:117–119.
357 González-Ferreiro, E., U. Diéguez-Aranda, and D. Miranda. 2012. Estimation of stand variables
358 in Pinus radiata D. Don plantations using different LiDAR pulse densities. Forestry 85:281–
359 292.
360 Gough, C. M., J. W. Atkins, R. T. Fahey, and B. S. Hardiman. 2019. High rates of primary
361 production in structurally complex forests. Ecology 100:e02864.
362 Guo, Q., Y. Su, T. Hu, H. Guan, S. Jin, J. Zhang, X. Zhao, K. Xu, D. Wei, M. Kelly, and N. C.
363 Coops. 2021, March 1. Lidar Boosts 3D Ecological Observations and Modelings: A Review
364 and Perspective. Institute of Electrical and Electronics Engineers Inc.
365 Hakkenberg, C. R., C. Song, R. K. Peet, and P. S. White. 2016. Forest structure as a predictor
366 of tree species diversity in the North Carolina Piedmont. Journal of Vegetation Science
367 27:1151–1163.

368 Huang, L., W. Xue, and T. Herben. 2019. Temporal niche differentiation among species
369 changes with habitat productivity and light conditions. Journal of Vegetation Science
370 30:438–447.
371 Jakubowski, M. K., Q. Guo, and M. Kelly. 2013. Tradeoffs between lidar pulse density and forest
372 measurement accuracy. Remote Sensing of Environment 130:245–253.
373 Kamoske, A. G., K. M. Dahlin, S. P. Serbin, and S. C. Stark. 2021. Leaf traits and canopy
374 structure together explain canopy functional diversity: an airborne remote sensing
375 approach. Ecological Applications 31:e02230.
376 Krause, K., and T. Goulden. 2015. NEON L0-TO-L1 DISCRETE RETURN LiDAR ALGORITHM
377 THEORETICAL BASIS DOCUMENT (ATBD) NEON.DOC.001291. Boulder, CO.
378 LaRue, E. A., B. S. Hardiman, J. M. Elliott, and S. Fei. 2019. Structural diversity as a predictor
379 of ecosystem function. Environmental Research Letters 14:114011.
380 LaRue, E. A., F. W. Wagner, S. Fei, J. W. Atkins, R. T. Fahey, C. M. Gough, and B. S.
381 Hardiman. 2020. Compatibility of Aerial and Terrestrial LiDAR for Quantifying Forest
382 Structural Diversity. Remote Sensing 12:1407.
383 Lefsky, M. A., W. B. Cohen, G. G. Parker, and D. J. Harding. 2002. LiDAR remote sensing for
384 ecosystem studies. Bioscience 52:19–30.
385 McCord, S. E., N. P. Webb, J. W. van Zee, S. H. Burnett, E. M. Christensen, E. M. Courtright, C.
386 M. Laney, C. Lunch, C. Maxwell, J. W. Karl, A. Slaughter, N. G. Stauffer, and C. Tweedie.
387 2021a. Provoking a Cultural Shift in Data Quality. BioScience 71:647–657.
388 McCord, S. E., J. L. Welty, J. Courtwright, C. Dillon, A. Traynor, S. H. Burnett, E. M. Courtright,
389 G. Fults, J. W. Karl, J. W. van Zee, N. P. Webb, and C. Tweedie. 2021b. Ten practical
390 questions to improve data quality. Rangelands In Press.
391 McCune, B., and J. Grace. 2002. Analysis of Ecological Communities. MjM Software, Gleneden
392 Beach, OR, USA.

McCune, B., and M. Mefford. 2006. PC-ORD. Multivariate Analysis of Ecological Data, Version 5.0 for Windows. MjM Software, Gleneden Beach, OR, USA.

Metzger, S., E. Ayres, D. Durden, C. Florian, R. Lee, C. Lunch, H. Luo, N. Pingintha-Durden, J. A. Roberti, M. SanClements, C. Sturtevant, K. Xu, and R. C. Zulueta. 2019. From NEON Field Sites to Data Portal: A Community Resource for Surface–Atmosphere Research Comes Online. Bulletin of the American Meteorological Society 100:2305–2325.

Michener, W. K. 2015. Ecological data sharing. Ecological Informatics 29:33–44.

Muggeo, V. 2008. segmented: an R Package to Fit Regression Models with Broken-Line Relationships. R News 8:20–25.

Nagy, C., and et al. 2021. Harnessing the NEON Data Revolution to Advance Open Environmental Science with a Diverse and Data-Capable Community. Ecosphere 12:e03833.

National Ecological Observatory Network. 2020. neonUtilities: Utilities for Working with NEON Data. R package version 1.3.3. https://CRAN.R-project.org/package=neonUtilities.

NEON. 2021a. (National Ecological Observatory Network). Discrete return LiDAR point cloud, RELEASE-2021 (DP1.30003.001). https://doi.org/10.48443/6e8k-3343. Dataset accessed from https://data.neonscience.org on April 23, 2021.

NEON. 2021b, September 28. Lidar https://www.neonscience.org/data-collection/lidar.

NEON. 2021c, December 20. National Ecological Observatory Network - Explore Field Sites.

Ouma, Y. O. 2016. Advancements in medium and high resolution Earth observation for land-surface imaging: Evolutions, future trends and contributions to sustainable development. Advances in Space Research 57:110–126.

Pearse, G. D., M. S. Watt, J. P. Dash, C. Stone, and G. Caccamo. 2019. Comparison of models describing forest inventory attributes using standard and voxel-based lidar predictors across a range of pulse densities. International Journal of Applied Earth Observation and Geoinformation 78:341–351.

Reichman, O. J., J. M. B, and S. M. P. 2011. Challenges and Opportunities of Open Data in Ecology. Science 331:703–705.

Roberti, D., A. de Almeida, S. Stark, C. Silva, C. Hamamura, and R. Valbuena. 2019. Calculates the Leaf Area Index (LAD) and Other Related Functions. CRAN.

Roussel, J. R., and D. Auty. 2018. LidR: Airborne LiDAR data manipulation and visualization for forestry applications. R package version 1:1.

Roussel, J. R., J. Caspersen, M. Béland, S. Thomas, and A. Achim. 2017. Removing bias from LiDAR-based estimates of canopy height: Accounting for the effects of pulse density and footprint size. Remote Sensing of Environment 198:1–16.

Ruiz, L. A., T. Hermosilla, F. Mauro, and M. Godino. 2014. Analysis of the influence of plot size and LiDAR density on forest structure attribute estimates. Forests 5:936–951.

Singh, K. K., G. Chen, J. B. McCarter, and R. K. Meentemeyer. 2015. Effects of LiDAR point density and landscape context on estimates of urban forest biomass. ISPRS Journal of Photogrammetry and Remote Sensing 101:310–322.

Spies, T. A., and J. F. Franklin. 1988. Old growth and forest dynamics in the Douglas-Fir region of Western Oregon and Washington. Natural Areas Journal 8:190–201.

Strunk, J., H. Temesgen, H. E. Andersen, J. P. Flewelling, and L. Madsen. 2012. Effects of lidar pulse density and sample size on a model-assisted approach to estimate forest inventory variables. Canadian Journal of Remote Sensing 38:644–654.

Treitz, P., K. Lim, M. Woods, D. Pitt, D. Nesbitt, and D. Etheridge. 2012. LiDAR sampling density for forest resource inventories in Ontario, Canada. Remote Sensing 4:830–848.

Wilkes, P., S. D. Jones, L. Suarez, A. Haywood, W. Woodgate, M. Soto-Berelov, A. Mellor, and A. K. Skidmore. 2015. Understanding the effects of als pulse density for metric retrieval across diverse forest types. Photogrammetric Engineering and Remote Sensing 81:625–635.

444 Yao, W., J. Krull, P. Krzystek, and M. Heurich. 2014. Sensitivity analysis of 3D individual tree
445 detection from LiDAR point clouds of temperate forests. Forests 5:1122–1142.
446 Yu, X., A. Kukko, H. Kaartinen, Y. Wang, X. Liang, L. Matikainen, and J. Hyyppä. 2020.
447 Comparing features of single and multi-photon lidar in boreal forests. ISPRS Journal of
448 Photogrammetry and Remote Sensing 168:268–276.
449 Zipkin, E. F., E. R. Zylstra, A. D. Wright, S. P. Saunders, A. O. Finley, M. C. Dietze, M. S. Itter,
450 and M. W. Tingley. 2021. Addressing data integration challenges to link ecological
451 processes across scales. Frontiers in Ecology and the Environment 19:30–38.
452

Preprints (www.preprints.org) | NOT PEER-REVIEWED | Posted: 23 December 2021 doi:10.20944/preprints202112.0390.v1

453 **Table 1.** Attributes of the forested NEON sites.

Attribute	Abby Road (ABBY)	Great Smoky Mountains (GRSM)	Steigerwaldt-Chequamegon (STEI)	University of Kansas Field Station (UKFS)	University of Notre Dame Environmental Research Center (UNDE)
Domain	Pacific Northwest	Appalachians and Cumberland Plateau	Great Lakes	Prairie Peninsula	Great Lakes
Latitude, longitude	45.762439, -122.330317	35.68896, -83.50195	45.50894, -89.58637	39.040431, -95.19215	46.23391, -89.537254
Forest type	Evergreen	Low elevation – deciduous, high elevation - evergreen	Mixed hardwoods	Mixed hardwoods	Second-growth northern mesic
Mean canopy height	34.0 m	30.0 m	20.0 m	19.0 m	24.0 m
Mean annual temperature	10.0 °C	13.1 °C	4.8 °C	12.7 °C	4.3 °C

454

Preprints (www.preprints.org) | NOT PEER-REVIEWED | Posted: 23 December 2021 doi:10.20944/preprints202112.0390.v1

455 **Table 2.** Stand-level forest structural diversity metrics estimated from NEON aerial LiDAR.

Category	Metric	Description
Height	MOCH	Mean of maximum height in 1m^2 grid of plot
	Q25	25th quantile of height
	Q50	50th quantile of height
	Q75	75th quantile of height
	Q100	Maximum canopy height
Density	VAI	Sum of the 1 m horizontal slices (starting 0.5 m above the ground) of leaf area density with the plot
Openness	DGF	Fraction of 1 m^2 canopy gaps in the plot
	GFP	Distribution of gaps in the point cloud 0.5 m above the ground
External heterogeneity	Rumple	Area of canopy surface relative to plot area
	Top rugosity	Standard deviation of outer canopy heights in 1 m^2 of plot
Internal heterogeneity	SD(ht)	Standard deviation of heights within the plot (m)
	SD(SD(ht))	Plot level- standard deviation of the standard deviation of heights within 9 m^2 voxels in the plot area (m)
	VCI	Normalization of diversity and evenness (entropy) of 1 m height bins within the plot
	CV(ht)	Coefficient of variation of heights within the plot
	FHD	Foliage height diversity
	Gini Index	Gini coefficient index

456

Preprints (www.preprints.org) | NOT PEER-REVIEWED | Posted: 23 December 2021 doi:10.20944/preprints202112.0390.v1

Table 3. The average point cloud density (change point) at which FSD metrics across different LiDAR plot densities stabilize at individual NEON forested sites and on average across all sites. The average change point from segmented regression (N_{Plots} = 40, $N_{Replicates/Density}$ = 5) at nine plots at each NEON site and FSD metric combination is shown, and the average minimum point density is based on an average across all sites.

Category	Metric	ABBY	GRSM	STEI	UKFS	UNDE	Average minimum point/m2
Height	MOCH	7.4 (1.0)	7.0 (0.9)	7.1 (0.7)	6.7 (0.1)	6.8 (0.9)	7.0
	q25	2.0 (0.0)	2.0 (0.0)	2.0 (0.0)	2.0 (0.0)	2.0 (0.0)	2.0
	q50	3.2 (2.3)	2.0 (0.0)	2.0 (0.0)	2.7 (2.0)	2.0 (0.0)	2.4
	q75	2.0 (0.0)	2.0 (0.0)	2.0 (0.0)	2.0 (0.0)	2.0 (0.0)	2.0
	q100	2.7 (2.0)	2.6 (1.9)	5.6 (5.3)	2.0 (0.0)	2.0 (0.0)	3.0
Density	VAI	2.0 (0.0)	2.0 (0.0)	2.0 (0.0)	2.0 (0.0)	2.0 (0.0)	2.0
Openness	DGF	5.6 (0.9)	4.8 (0.6)	5.3 (0.8)	5.1 (0.7)	4.9 (0.6)	5.1
	GFP	2.0 (0.0)	2.0 (0.0)	2.7 (2.0)	2.0 (0.0)	3.1 (2.2)	2.3
	Rumple	7.3 (0.8)	7.0 (0.7)	7.0 (0.6)	6.9 (0.6)	6.8 (0.2)	7.0

Preprints (www.preprints.org) | NOT PEER-REVIEWED | Posted: 23 December 2021 doi:10.20944/preprints202112.0390.v1

External heterogeneity	**Top Rugosity**	8.1 (1.0)	7.8 (1.1)	7.1 (1.1)	7.5 (1.0)	7.0 (1.3)	7.5
Internal heterogeneity	**SD(ht)**	2.0 (0.0)	2.0 (0.0)	2.0 (0.0)	2.0 (0.0)	2.0 (0.0)	2.0
	SDSD(ht)	5.5 (2.2)	6.6 (1.1)	5.6 (0.9)	5.8 (1.1)	5.5 (1.1)	5.8
	VCI	2.0 (0.0)	2.0 (0.0)	2.0 (0.0)	2.4 (1.1)	2.0 (0.0)	2.1
	CV(ht)	2.2 (0.7)	2.0 (0.0)	2.0 (0.0)	2.5 (1.6)	2.0 (0.0)	2.2
	FHD	7.1 (4.2)	4.3 (2.0)	3.5 (3.0)	4.2 (2.3)	4.4 (2.0)	4.7
	Gini Index	2.2 (0.7)	2.0 (0.0)	2.0 (0.0)	2.5 (1.6)	2.0 (0.0)	2.2

461

Preprints (www.preprints.org) | NOT PEER-REVIEWED | Posted: 23 December 2021 doi:10.20944/preprints202112.0390.v1

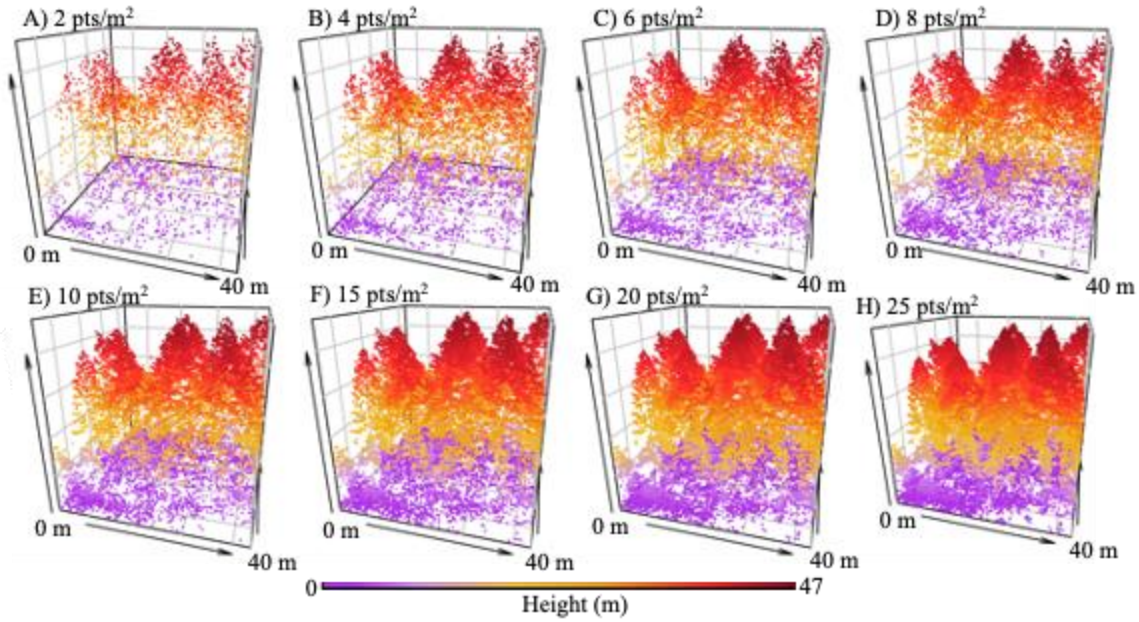

462

463 **Figure 1.** Simulated LiDAR point densities from a 40 x 40 m NEON base plot at Abby Road

464 (ABBY_029), a NEON site in the Pacific Northwest of the USA.

Preprints (www.preprints.org) | NOT PEER-REVIEWED | Posted: 23 December 2021 doi:10.20944/preprints202112.0390.v1

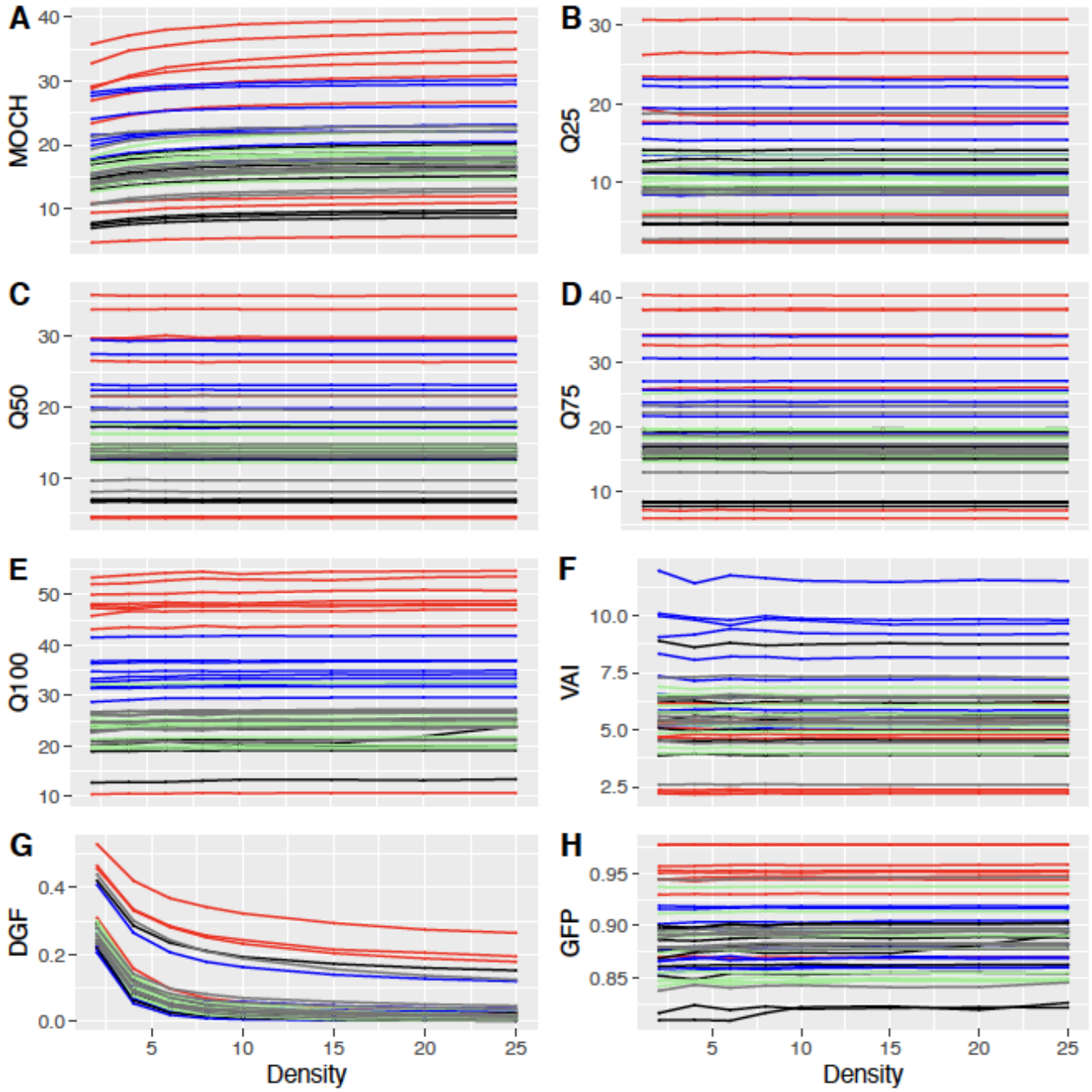

Figure 2. Height, density, and cover and openness structural diversity metrics across different NEON LiDAR point densities (see Table 2 for metric definitions). The point value for each plot at a unique point density is the average of the 5 randomly thinned replicates. Line shading indicates the site (red – ABBY, blue – GRSM, black – STEI, green – UKFS, gray – UNDE).

Preprints (www.preprints.org) | NOT PEER-REVIEWED | Posted: 23 December 2021 doi:10.20944/preprints202112.0390.v1

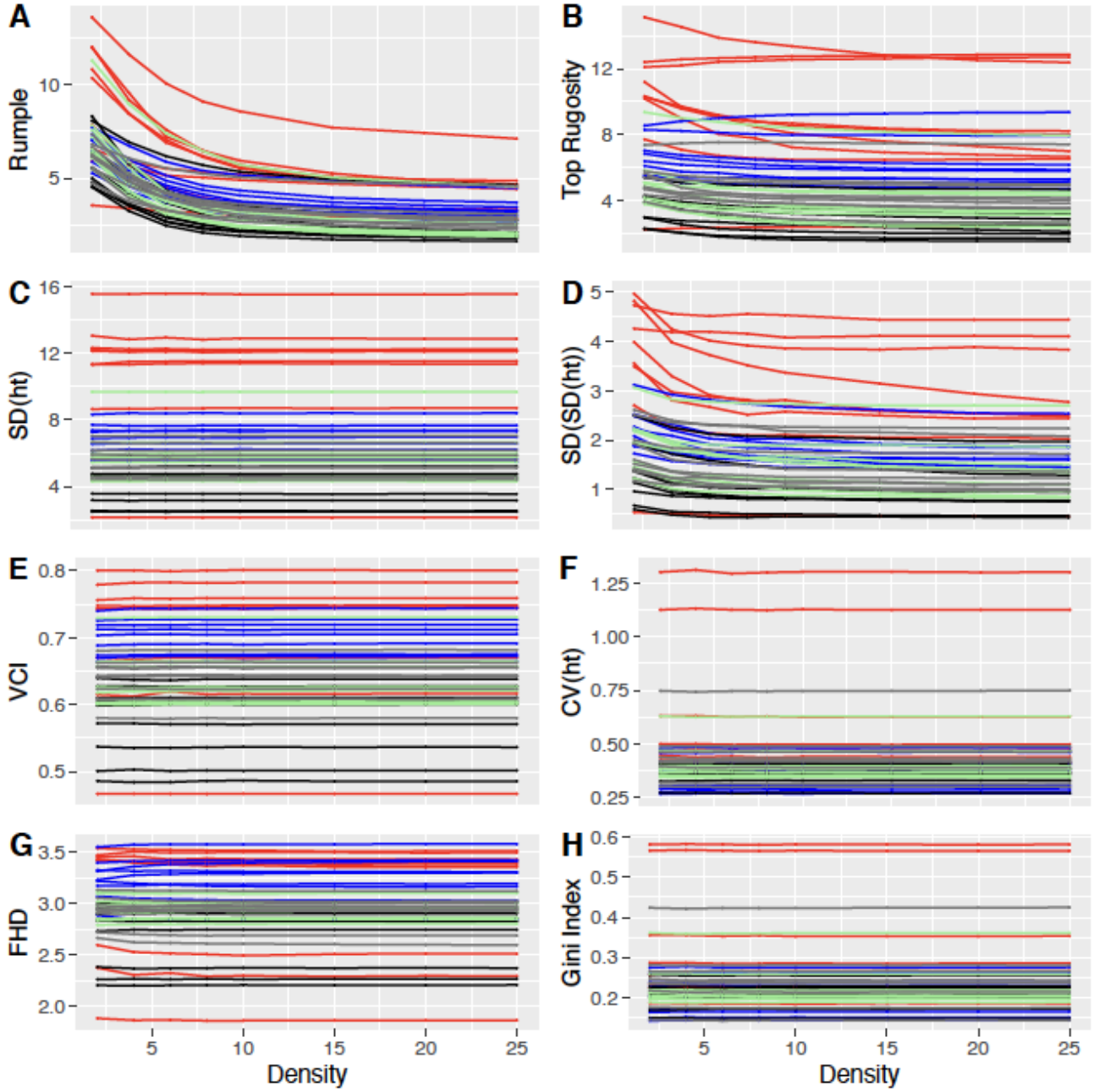

Figure 3. External and internal heterogeneity structural diversity metrics across different NEON LiDAR point densities (see Table 2 for metric definitions). The point value for each plot at a unique point density is the average of the 5 randomly thinned replicates. Line shading indicates the site (red – ABBY, blue – GRSM, black – STEI, green – UKFS, gray – UNDE).

Preprints (www.preprints.org) | NOT PEER-REVIEWED | Posted: 23 December 2021 doi:10.20944/preprints202112.0390.v1

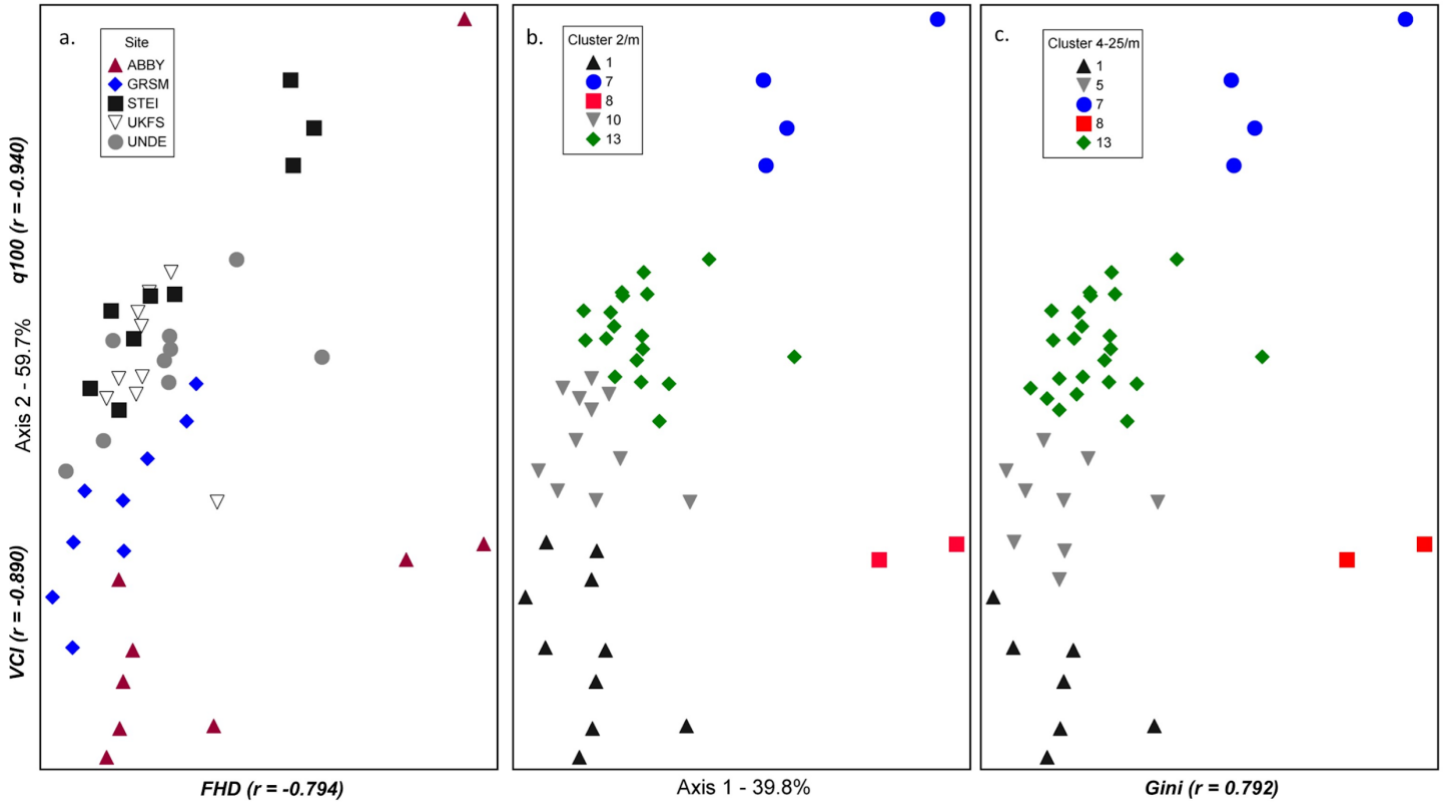

Figure 4. Illustration of relationships among plots in structural diversity space based on nonmetric multi-dimensional (NMS) scaling ordination and delineation into structural complexity types using hierarchical agglomerative clustering. Each panel illustrates ordination using 10 points/m^2 spacing, but each panel shows a different grouping of plots based on: A) site, B) hierarchical clustering of plots based on structural type composition for 2 points/m^2 spacing, and B) clustering of plots for 4-25 points/m^2 spacing levels which had equivalent grouping of plots into clusters. Structural diversity metrics most strongly correlated with ordination axes are indicated along both axes along with correlation coefficients (see Table 2 for metric definitions).

Preprints (www.preprints.org) | NOT PEER-REVIEWED | Posted: 23 December 2021 doi:10.20944/preprints202112.0390.v1

Appendix S1.

Table S1. The point cloud density (change point) at which FSD metrics across different LiDAR plot densities stabilize. The change point from segmented regression (N_{Plots} = 40, $N_{Replicates/Density}$ = 5) at plots at each NEON site and FSD metric combination is shown. A 2.0 pt/m^2 is displayed if the pseudo score statistic test had an $\alpha > 0.05$ after correcting for multiple comparisons with FDR (N_{Tests} = 720).

Site	Plot ID	MOCH	q25	q50	q75	q100	VAI	DGP	GFP	Rumple	Top Rugosity	SD(ht)	SDSD(ht)	VCI	CV(ht)	FHD	Gini Index
ABBY	ABBY_001	6.7	2.0	2.0	2.0	2.0	2.0	6.3	2.0	7.2	7.0	2.0	4.8	2.0	2.0	6.6	2.0
ABBY	ABBY_006	6.7	2.0	2.0	2.0	2.0	2.0	4.7	2.0	6.8	6.7	2.0	4.5	2.0	2.0	2.0	2.0
ABBY	ABBY_014	6.8	2.0	2.0	2.0	2.0	2.0	4.8	2.0	6.8	8.7	2.0	4.7	2.0	2.0	2.0	2.0
ABBY	ABBY_016	6.8	2.0	2.0	2.0	2.0	2.0	6.1	2.0	7.0	8.4	2.0	5.2	2.0	2.0	5.3	2.0
ABBY	ABBY_025	6.8	2.0	8.0	2.0	2.0	2.0	4.5	2.0	6.6	6.7	2.0	4.5	2.0	2.0	13.7	2.0
ABBY	ABBY_029	8.6	2.0	6.4	2.0	2.0	2.0	4.7	2.0	8.6	9.0	2.0	6.1	2.0	4.2	13.5	4.2
ABBY	ABBY_062	8.5	2.0	2.0	2.0	8.0	2.0	6.4	2.0	8.9	8.8	2.0	7.5	2.0	2.0	6.9	2.0
ABBY	ABBY_068	6.5	2.0	2.0	2.0	2.0	2.0	6.4	2.0	6.6	8.6	2.0	10.0	2.0	2.0	6.3	2.0
ABBY	ABBY_073	8.9	2.0	2.0	2.0	2.0	2.0	6.4	2.0	7.0	8.7	2.0	2.0	2.0	2.0	7.3	2.0
GRSM	GRSM_004	7.0	2.0	2.0	2.0	2.0	2.0	4.5	2.0	6.9	6.4	2.0	8.3	2.0	2.0	2.0	2.0
GRSM	GRSM_006	6.8	2.0	2.0	2.0	2.0	2.0	4.5	2.0	6.9	8.8	2.0	7.2	2.0	2.0	2.0	2.0
GRSM	GRSM_012	6.8	2.0	2.0	2.0	2.0	2.0	4.6	2.0	6.5	9.0	2.0	6.5	2.0	2.0	5.1	2.0
GRSM	GRSM_016	6.7	2.0	2.0	2.0	2.0	2.0	4.6	2.0	6.7	7.3	2.0	5.1	2.0	2.0	6.9	2.0
GRSM	GRSM_026	8.6	2.0	2.0	2.0	2.0	2.0	4.7	2.0	7.0	8.7	2.0	4.6	2.0	2.0	7.3	2.0
GRSM	GRSM_029	6.8	2.0	2.0	2.0	2.0	2.0	4.7	2.0	6.5	6.9	2.0	7.1	2.0	2.0	4.3	2.0
GRSM	GRSM_050	8.5	2.0	2.0	2.0	2.0	2.0	4.8	2.0	8.8	9.0	2.0	6.4	2.0	2.0	4.2	2.0
GRSM	GRSM_056	5.6	2.0	2.0	2.0	2.0	2.0	6.3	2.0	7.1	7.1	2.0	7.1	2.0	2.0	2.0	2.0
GRSM	GRSM_060	6.6	2.0	2.0	2.0	7.8	2.0	4.6	2.0	6.8	6.9	2.0	7.0	2.0	2.0	4.5	2.0
STEI	STEI_003	6.7	2.0	2.0	2.0	2.0	2.0	4.5	2.0	6.5	6.4	2.0	6.3	2.0	2.0	2.0	2.0
STEI	STEI_006	6.8	2.0	2.0	2.0	2.0	2.0	6.1	7.9	6.9	6.9	2.0	7.0	2.0	2.0	2.0	2.0
STEI	STEI_009	6.7	2.0	2.0	2.0	2.0	2.0	4.6	2.0	6.8	6.7	2.0	6.3	2.0	2.0	9.8	2.0
STEI	STEI_015	6.6	2.0	2.0	2.0	4.6	2.0	6.3	2.0	8.5	4.9	2.0	5.2	2.0	2.0	7.9	2.0
STEI	STEI_018	6.8	2.0	2.0	2.0	9.1	2.0	4.7	2.0	7.0	7.4	2.0	4.9	2.0	2.0	2.0	2.0
STEI	STEI_046	8.2	2.0	2.0	2.0	16.7	2.0	6.2	2.0	7.0	8.3	2.0	4.6	2.0	2.0	2.0	2.0
STEI	STEI_050	6.9	2.0	2.0	2.0	2.0	2.0	4.7	2.0	6.7	6.4	2.0	6.3	2.0	2.0	2.0	2.0
STEI	STEI_054	8.3	2.0	2.0	2.0	2.0	2.0	6.1	2.0	6.8	8.3	2.0	5.0	2.0	2.0	2.0	2.0
STEI	STEI_062	7.0	2.0	2.0	2.0	10.0	2.0	4.7	2.0	6.8	8.3	2.0	4.7	2.0	2.0	2.0	2.0
UKFS	UKFS_002	6.8	2.0	8.0	2.0	2.0	2.0	4.6	2.0	6.7	6.6	2.0	4.7	5.3	6.8	5.4	6.7
UKFS	UKFS_007	6.8	2.0	2.0	2.0	2.0	2.0	6.2	2.0	8.5	9.0	2.0	4.5	2.0	2.0	2.0	2.0
UKFS	UKFS_014	6.8	2.0	2.0	2.0	2.0	2.0	4.7	2.0	7.0	7.1	2.0	6.3	2.0	2.0	4.2	2.0
UKFS	UKFS_021	6.7	2.0	2.0	2.0	2.0	2.0	4.6	2.0	6.6	9.0	2.0	5.1	2.0	2.0	2.0	2.0
UKFS	UKFS_043	6.7	2.0	2.0	2.0	2.0	2.0	4.8	2.0	6.5	6.7	2.0	6.6	2.0	2.0	6.3	2.0
UKFS	UKFS_047	6.7	2.0	2.0	2.0	2.0	2.0	4.6	2.0	6.6	6.9	2.0	7.1	2.0	2.0	2.0	2.0
UKFS	UKFS_052	6.8	2.0	2.0	2.0	2.0	2.0	6.1	2.0	6.8	8.5	2.0	6.8	2.0	2.0	6.3	2.0
UKFS	UKFS_054	6.7	2.0	2.0	2.0	2.0	2.0	4.6	2.0	6.7	6.7	2.0	6.7	2.0	2.0	8.0	2.0
UKFS	UKFS_059	6.6	2.0	2.0	2.0	2.0	2.0	6.1	2.0	6.8	6.7	2.0	4.6	2.0	2.0	2.0	2.0
UNDE	UNDE_003	6.8	2.0	2.0	2.0	2.0	2.0	4.7	2.0	7.0	7.5	2.0	4.4	2.0	2.0	5.1	2.0
UNDE	UNDE_016	8.8	2.0	2.0	2.0	2.0	2.0	6.5	2.0	7.0	5.1	2.0	4.6	2.0	2.0	4.4	2.0
UNDE	UNDE_020	6.9	2.0	2.0	2.0	2.0	2.0	4.6	2.0	7.0	9.0	2.0	6.6	2.0	2.0	4.3	2.0
UNDE	UNDE_027	6.7	2.0	2.0	2.0	2.0	2.0	4.6	2.0	6.5	6.9	2.0	6.4	2.0	2.0	6.6	2.0
UNDE	UNDE_037	6.7	2.0	2.0	2.0	2.0	2.0	4.6	2.0	6.7	6.7	2.0	6.9	2.0	2.0	6.6	2.0
UNDE	UNDE_043	5.0	2.0	2.0	2.0	2.0	2.0	4.6	2.0	6.6	4.9	2.0	4.6	2.0	2.0	2.0	2.0
UNDE	UNDE_049	6.9	2.0	2.0	2.0	2.0	2.0	4.8	6.2	7.2	7.1	2.0	4.7	2.0	2.0	6.2	2.0
UNDE	UNDE_055	6.7	2.0	2.0	2.0	2.0	2.0	4.7	2.0	6.7	7.3	2.0	4.7	2.0	2.0	2.0	2.0
UNDE	UNDE_057	6.8	2.0	2.0	2.0	2.0	2.0	4.7	7.6	6.7	8.4	2.0	6.6	2.0	2.0	2.0	2.0